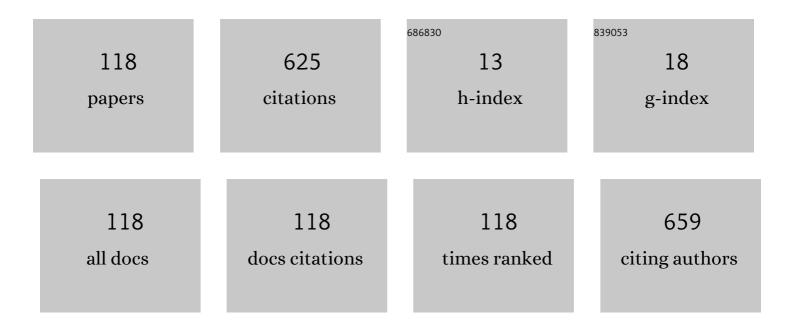
Pavel A Yunin

List of Publications by Year in descending order

Source: https://exaly.com/author-pdf/996106/publications.pdf Version: 2024-02-01



ΔΑΛΙΕΙ Δ ΥΠΝΙΝ

#	Article	IF	CITATIONS
1	Homoepitaxial growth of CVD diamond after ICP pretreatment. Physica Status Solidi (A) Applications and Materials Science, 2015, 212, 2572-2577.	0.8	27
2	Sputter depth profiling of Mo/B4C/Si and Mo/Si multilayer nanostructures: A round-robin characterization by different techniques. Thin Solid Films, 2013, 540, 96-105.	0.8	24
3	Monolithically integrated InGaAs/GaAs/AlGaAs quantum well laser grown by MOCVD on exact Ge/Si(001) substrate. Applied Physics Letters, 2016, 109, .	1.5	24
4	Impact of growth and annealing conditions on the parameters of Ge/Si(001) relaxed layers grown by molecular beam epitaxy. Semiconductors, 2015, 49, 1415-1420.	0.2	23
5	Towards the indium nitride laser: obtaining infrared stimulated emission from planar monocrystalline InN structures. Scientific Reports, 2018, 8, 9454.	1.6	21
6	GaAs/Ge/Si epitaxial substrates: Development and characteristics. AIP Advances, 2017, 7, .	0.6	20
7	Graft and block copolymers of chitosan with vinyl monomers: Synthesis, structure, and properties. Polymer Science - Series B, 2015, 57, 93-105.	0.3	17
8	Characterization of interfaces in mosaic CVD diamond crystal. Journal of Crystal Growth, 2016, 442, 62-67.	0.7	17
9	Copper(II)–cerium(III) 15-metallacrown-5 based on glycinehydroxamic acid as a new precursor for heterobimetallic composite materials on carbon nanotubes. Polyhedron, 2016, 114, 96-100.	1.0	17
10	YBa ₂ Cu ₃ O _{7â^'Î} long Josephson junctions on bicrystal Zr _{1â^'x} Y _x O ₂ substrates fabricated by preliminary topology masks. Superconductor Science and Technology, 2017, 30, 025007.	1.8	16
11	The role of ultra-thin carbon barrier layers for fabrication of La/B4C interferential mirrors: Study by time-of-flight secondary ion mass spectrometry and high-resolution transmission electron microscopy. Thin Solid Films, 2015, 577, 11-16.	0.8	15
12	Features of spectral properties of Sm3+ complexes with dithia- and diselenophosphinate ligands. Spectrochimica Acta - Part A: Molecular and Biomolecular Spectroscopy, 2016, 163, 134-139.	2.0	15
13	Kinetics and formation mechanism of yttrium aluminum garnet from an amorphous phase prepared by the sol–gel method. Ceramics International, 2015, 41, 10616-10623.	2.3	14
14	Terahertz radiation from bismuth surface induced by femtosecond laser pulses. Optics Letters, 2016, 41, 4289.	1.7	14
15	Experimental shift allowance in the deconvolution of SIMS depth profiles. Surface and Interface Analysis, 2013, 45, 1228-1232.	0.8	13
16	Recovery of SIMS depth profiles with account for nonstationary effects. Applied Surface Science, 2014, 307, 33-41.	3.1	13
17	A new approach to express ToF SIMS depth profiling. Surface and Interface Analysis, 2015, 47, 771-776.	0.8	12
18	Phase transitions in hybrid SFS structures with thin superconducting layers. JETP Letters, 2016, 104, 329-333.	0.4	12

#	Article	IF	CITATIONS
19	New hybrid material based on multiwalled carbon nanotubes decorated with rhenium nanoparticles. Journal of Surface Investigation, 2015, 9, 694-698.	0.1	11
20	MOCVD Growth of InGaAs/GaAs/AlGaAs Laser Structures with Quantum Wells on Ge/Si Substrates. Crystals, 2018, 8, 311.	1.0	11
21	Peculiarities in magnetron sputtering of YBCO epitaxial films for applications in superconductor electronics devices. Technical Physics, 2015, 60, 1682-1688.	0.2	10
22	Pyrolytic deposition of nanostructured titanium carbide coatings on the surface of multiwalled carbon nanotubes. Technical Physics Letters, 2016, 42, 517-519.	0.2	10
23	Si3N4 layers for the in-situ passivation of GaN-based HEMT structures. Semiconductors, 2015, 49, 1421-1424.	0.2	9
24	A study of planar structures formed on the modified Al2O3 surfaces determining the topology of superconducting elements during YBa2Cu3O7–d deposition. Technical Physics Letters, 2016, 42, 594-597.	0.2	9
25	Depth profiling of fullerene-containing structures by time-of-flight secondary ion mass spectrometry. Technical Physics Letters, 2013, 39, 1097-1100.	0.2	8
26	The Gas-Phase Synthesis of a New Functional Hybrid Material on the Basis of Multiwalled Carbon Nanotubes Decorated with Faceted Aluminum Nanocrystals. Technical Physics Letters, 2018, 44, 865-868.	0.2	8
27	Matched characterization of super-multiperiod superlattices. Journal Physics D: Applied Physics, 2020, 53, 455103.	1.3	8
28	A new approach to the diagnostics of nanoislands in Ge x Si1 â^' x /Si heterostructures by secondary ion mass spectrometry. Technical Physics Letters, 2014, 40, 601-605.	0.2	7
29	Structural and optical properties of GaAsSb QW heterostructures grown by laser deposition. Semiconductors, 2015, 49, 109-112.	0.2	7
30	Electrical conductivity of vacuum deposited films and crystals of redox-isomeric о-semiquinonato cobalt complexes. Solid State Sciences, 2015, 48, 13-18.	1.5	7
31	Grazing incidence mirrors with enhanced reflectance in the soft X-ray region. Thin Solid Films, 2016, 598, 156-160.	0.8	7
32	Influence of thermal annealing on the electrical and luminescent properties of heavily Sb-doped Ge/Si(001) layers. Semiconductor Science and Technology, 2018, 33, 124019.	1.0	7
33	Method for taking into account the shift parameter in the deconvolution of the depth composition distribution of semiconductor structures from SIMS depth profiles. Semiconductors, 2012, 46, 1481-1486.	0.2	6
34	Thin single-crystal Ge layers on 2″ Si substrates. Technical Physics Letters, 2015, 41, 36-39.	0.2	6
35	Features of InN growth by nitrogen-plasma-assisted MBE at different ratios of fluxes of group-III and -V elements. Semiconductors, 2016, 50, 261-265.	0.2	6
36	Quantitative depth profiling of Si1–xGex structures by time-of-flight secondary ion mass spectrometry and secondary neutral mass spectrometry. Thin Solid Films, 2016, 607, 25-31.	0.8	6

#	Article	IF	CITATIONS
37	Hydrogen reduction of 98MoF6 in RF discharge. Journal of Radioanalytical and Nuclear Chemistry, 2016, 309, 833.	0.7	6
38	InN Layers Grown by MOCVD on <i>a</i> â€Plane Al ₂ O ₃ . Physica Status Solidi (A) Applications and Materials Science, 2018, 215, 1700919.	0.8	6
39	Study of the Structural and Morphological Properties of HPHT Diamond Substrates. Semiconductors, 2018, 52, 1432-1436.	0.2	6
40	Quantitative calibration and germanium SIMS depth profiling in Ge x Si1 â^ x /Si heterostructures. Semiconductors, 2014, 48, 1109-1117.	0.2	5
41	Continuous monitoring of temperature and rate of plasma etching of semiconductor wafers. Applied Physics Letters, 2015, 107, .	1.5	5
42	Peculiarities of growing InGaAs/GaAs/AlGaAs laser structures by MOCVD on Ge/Si substrates. Semiconductors, 2017, 51, 1527-1530.	0.2	5
43	Synchrotron, X-Ray, and Electron Microscopic Studies of Catalyst Systems Based on Multiwalled Carbon Nanotubes Modified by Copper Nanoparticles. Physics of the Solid State, 2020, 62, 214-222.	0.2	5
44	Near-infrared stimulated emission from indium-rich InGaN layers grown by plasma-assisted MBE. Applied Physics Letters, 2021, 118, .	1.5	5
45	Study of multilayered SiGe semiconductor structures by X-ray diffractometry, grazing-incidence X-ray reflectometry, and secondary-ion mass spectrometry. Semiconductors, 2013, 47, 1556-1561.	0.2	4
46	Growth and formation of the microstructure of YBCO films deposited by magnetron sputtering on fianite substrates. Technical Physics, 2014, 59, 1487-1491.	0.2	4
47	Raman spectra of amorphous isotope-enriched 74Ge with low-strained Ge nanocrystals. Thin Solid Films, 2014, 552, 46-49.	0.8	4
48	Synthesis and properties of chitosan-polylactide compositions produced with the use of compatibilizers. Polymer Science - Series B, 2015, 57, 239-243.	0.3	4
49	Phase Diagrams of Thin Disordered Films Based on HTSC YBa2Cu3O7–Âx in External Magnetic Fields. Physics of the Solid State, 2019, 61, 1523-1528.	0.2	4
50	SIMS Analysis of Carbon-Containing Materials: Content of Carbon Atoms in sp2 and sp3 Hybridization States. Technical Physics Letters, 2020, 46, 290-294.	0.2	4
51	A new alternative to secondary CsM+ ions for depth profiling of multilayer metal structures by secondary ion mass spectrometry. Technical Physics Letters, 2013, 39, 46-50.	0.2	3
52	Monocrystalline InN Films Grown at High Rate by Organometallic Vapor Phase Epitaxy with Nitrogen Plasma Activation Supported by Gyrotron Radiation. Japanese Journal of Applied Physics, 2013, 52, 110201.	0.8	3
53	Use of related parameters in X-ray diffraction analysis of multilayer structures with allowance for the layer growth time. Technical Physics, 2014, 59, 402-406.	0.2	3
54	Growth of light-emitting SiGe heterostructures on strained silicon-on-insulator substrates with a thin oxide layer. Semiconductors, 2015, 49, 1104-1110.	0.2	3

#	Article	IF	CITATIONS
55	Formation of singular (001) terraces on the surface of single-crystal HPHT diamond substrates. Semiconductors, 2016, 50, 1622-1625.	0.2	3
56	Heavily doped GaAs:Te layers grown by MOVPE using diisopropyl telluride as a source. Semiconductors, 2016, 50, 1439-1442.	0.2	3
57	On the use of an external reference sample in the X-ray diffraction analysis of epitaxial layers. Journal of Surface Investigation, 2016, 10, 96-100.	0.1	3
58	A Study of the Isolation Region of Planar Superconducting YBCO Structures Formed by the Master Mask Method. Physics of the Solid State, 2018, 60, 2139-2144.	0.2	3
59	On the Application of Strain-Compensating GaAsP Layers for the Growth of InGaAs/GaAs Quantum-Well Laser Heterostructures Emitting at Wavelengths above 1100 nm on Artificial Ge/Si Substrates. Semiconductors, 2018, 52, 1547-1550.	0.2	3
60	A Comparative Analysis of Catalysts for the Preparation of Germanium through Hydrogen Reduction of Germanium Tetrachloride. Inorganic Materials, 2018, 54, 971-976.	0.2	3
61	Plasma-Chemical Deposition of Diamond-Like Films onto the Surface of Heavily Doped Single-Crystal Diamond. Semiconductors, 2019, 53, 1203-1206.	0.2	3
62	Misorientation Angle Dependence of Boron Incorporation Into CVD Diamond Delta Layers. Physica Status Solidi (B): Basic Research, 2019, 256, 1800606.	0.7	3
63	Influence of Thermal Annealing on the Properties of Multilayer Mo/Be Mirrors. Technical Physics, 2019, 64, 1692-1697.	0.2	3
64	Experimental Observation of s-Component of Superconducting Pairing in Thin Disordered HTSC Films Based on YBCO. Physics of the Solid State, 2020, 62, 1598-1603.	0.2	3
65	Small-molecule heterojunctions: Stability to ageing under sunlight. Applied Surface Science, 2022, 578, 152084.	3.1	3
66	Ion-Beam Synthesis of Gallium Oxide Nanocrystals in a SiO2/Si Dielectric Matrix. Nanomaterials, 2022, 12, 1840.	1.9	3
67	Direct comparison of superlattice periods measured with X-ray diffractometry and optical interferometry. Bulletin of the Russian Academy of Sciences: Physics, 2011, 75, 40-43.	0.1	2
68	Layer-by-layer analysis of structures containing δ-layers by secondary ion mass spectrometry taking into account the TOF.SIMS-5 depth resolution function. Journal of Surface Investigation, 2012, 6, 574-577.	0.1	2
69	Analysis of the composition of (Al,Ga)As alloys by secondary ion mass spectroscopy and X-ray diffractometry. Semiconductors, 2012, 46, 1392-1395.	0.2	2
70	New approach to the X-ray diffraction analysis of test structures during flow calibration in epitaxial growth reactors. Journal of Surface Investigation, 2012, 6, 494-497.	0.1	2
71	The waveguide effect of InGaAs quantum wells in a GaAs structure on Si substrate with Ge buffer layer. Technical Physics Letters, 2015, 41, 648-650.	0.2	2
72	Application of a pseudomorphous layer on a vicinal substrate as a test sample for high-resolution X-ray diffractometry. Journal of Surface Investigation, 2015, 9, 1243-1250.	0.1	2

#	Article	IF	CITATIONS
73	Raman spectroscopy of InGaAs/GaAs nanoheterostructures δ-doped with Mn. Semiconductors, 2015, 49, 99-103.	0.2	2
74	Modification of YBa2Cu3O7–δthin films by ion implantation. Journal of Surface Investigation, 2016, 10, 438-440.	0.1	2
75	Nonlinear calibration curves in secondary ion mass spectrometry for quantitative analysis of gesi heterostructures with nanoclusters. Technical Physics Letters, 2016, 42, 243-247.	0.2	2
76	Epitaxial GaN layers formed on langasite substrates by the plasma-assisted MBE method. Semiconductors, 2016, 50, 1511-1514.	0.2	2
77	Grazing Incidence X-Ray Diffraction Study of Tantalum Thin Films. Journal of Surface Investigation, 2018, 12, 701-704.	0.1	2
78	New Hybrid Material Based on Multiwalled Carbon Nanotubes Decorated by Rhenium-Tungsten Nanodendrites. Journal of Surface Investigation, 2018, 12, 682-687.	0.1	2
79	Emission Properties of Heavily Doped Epitaxial Indium-Nitride Layers. Semiconductors, 2019, 53, 1357-1362.	0.2	2
80	Carbon Films Produced by the Pulsed Laser Method and Their Influence on the Properties of GaAs Structures. Semiconductors, 2020, 54, 1059-1063.	0.2	2
81	Effect of antimony doping on the energy of optical transitions in n-Ge layers grown on Si (001) and Ge (001) substrates. Journal of Applied Physics, 2020, 127, 165701.	1.1	2
82	Nanostructuring of Mn(II)Pc thin films by vacuum deposition in a weak magnetic field. Vacuum, 2021, 194, 110584.	1.6	2
83	Changes in the elemental composition and microstructure of an YBa2Cu3O7 â^ Î^ target during magnetron sputtering. Technical Physics Letters, 2013, 39, 862-865.	0.2	1
84	High-rate growth of InN films on fianite and sapphire substrates by metalorganic vapor phase epitaxy with plasma-assisted nitrogen activation. Technical Physics Letters, 2015, 41, 266-269.	0.2	1
85	Influence of surface roughness on a change in the growth mode from two-dimensional to three-dimensional for strained SiGe heterostructures. Semiconductors, 2016, 50, 1630-1634.	0.2	1
86	High-coercivity magnetic mirror polarizers for thermal neutrons. Journal of Surface Investigation, 2016, 10, 486-489.	0.1	1
87	Investigation of X-ray diffraction limitations upon the analysis of tellurium-atom injection into GaAs epitaxial layers. Journal of Surface Investigation, 2017, 11, 361-365.	0.1	1
88	Selective analysis of the elemental composition of InGaAs/GaAs nanoclusters by secondary ion mass spectrometry. Technical Physics Letters, 2017, 43, 477-480.	0.2	1
89	Low-temperature deposition of SiNx Films in SiH4/Ar + N2 inductively coupled plasma under high silane dilution with argon. Semiconductors, 2017, 51, 1449-1452.	0.2	1
90	Synthesis of Hybrid Materials Based on Iron Nanoparticle-Decorated Multiwalled Carbon Nanotubes. Inorganic Materials, 2018, 54, 233-236.	0.2	1

#	Article	IF	CITATIONS
91	Investigation of the Anisotropy of the Structural Properties of GaN(0001) Layers Grown by MOVPE on a-Plane (11 \$\$ar {2}\$\$ 0) Sapphire. Semiconductors, 2018, 52, 1412-1415.	0.2	1
92	Plasma Chemical Etching of Gallium Arsenide in C2F5Cl-Based Inductively Coupled Plasma. Semiconductors, 2018, 52, 1473-1476.	0.2	1
93	A New Limitation of the Depth Resolution in TOF-SIMS Elemental Profiling: the Influence of a Probing Ion Beam. Technical Physics Letters, 2018, 44, 320-323.	0.2	1
94	New Cluster Secondary lons for Quantitative Analysis of the Concentration of Boron Atoms in Diamond by Time-of-Flight Secondary-lon Mass Spectrometry. Technical Physics Letters, 2018, 44, 297-300.	0.2	1
95	Influence of the Rotation Frequency of a Disk Substrate Holder on the Crystal Structure Characteristics of MOCVD-Grown GaAs Layers. Technical Physics, 2018, 63, 211-215.	0.2	1
96	Comparative Analysis of the Luminescence of Ge:Sb Layers Grown on Ge(001) and Si(001) Substrates. Semiconductors, 2019, 53, 1318-1323.	0.2	1
97	Pulsed Ion-Beam Treatment of Germanium Implanted by Antimony Ions. Optoelectronics, Instrumentation and Data Processing, 2019, 55, 423-430.	0.2	1
98	Magnetostriction Effect in Ferromagnetic Films with Easy-Axis and Easy-Plane Anisotropies. Technical Physics, 2019, 64, 1646-1651.	0.2	1
99	Low-barrier Mott diodes with near-surface polarization-induced <i>δ</i> -doping. Applied Physics Letters, 2020, 116, .	1.5	1
100	Formation of Ohmic Contacts to a Diamond-Like Carbon Layer Deposited on a Dielectric Diamond Substrate. Semiconductors, 2020, 54, 1056-1058.	0.2	1
101	Possibilities of the Master Mask Method in Analysis of Characteristics of Planar HTSC Structures Depending on Superconducting Film Thickness. Technical Physics, 2020, 65, 1605-1608.	0.2	1
102	The Microstructure of Transition Boundaries in Multilayer Mo/Be Systems. Technical Physics, 2020, 65, 1800-1808.	0.2	1
103	Effect of the AlGaAs Seed Layer Composition on Antiphase Domains Formation in (Al)GaAs Structures Grown by Vapor-Phase Epitaxy on Ge/Si(100) Substrates. Technical Physics Letters, 2021, 47, 413-416.	0.2	1
104	Coulomb centers assisted tunneling in a δ-doped triple barrier SiGe heterostructure. Physica E: Low-Dimensional Systems and Nanostructures, 2014, 57, 42-46.	1.3	0
105	Single-crystal GaN/AIN layers on CVD diamond. Technical Physics Letters, 2015, 41, 954-956.	0.2	0
106	Terahertz-range spontaneous emission under the optical excitation of donors in uniaxially stressed bulk silicon and SiGe/Si heterostructures. Semiconductors, 2015, 49, 13-18.	0.2	0
107	Plastic relaxation in GeSi layers on Si (001) and Si (115) substrates. Semiconductors, 2015, 49, 19-22.	0.2	0
108	Extremely deep profiling analysis of the atomic composition of thick (>100 μm) GaAs layers within power PIN diodes by secondary ion mass spectrometry. Technical Physics Letters, 2016, 42, 783-787.	0.2	0

#	ARTICLE	IF	CITATIONS
109	Stimulated emission from a metamorphic GaAsSb bulk layer on a GaAs substrate. Semiconductors, 2016, 50, 586-589.	0.2	0
110	Specific features of the photoexcitation spectra of epitaxial InN layers grown by molecular-beam epitaxy with the plasma activation of nitrogen. Semiconductors, 2017, 51, 1537-1541.	0.2	0
111	Mechanisms of optical-to-THz conversion on metal and semimetal surfaces. AIP Conference Proceedings, 2017, , .	0.3	0
112	Verification of the Hypothesis on the Thermoelastic Nature of Deformation of a (0001)GaN Layer Grown on the Sapphire a-Cut. Semiconductors, 2018, 52, 1491-1494.	0.2	0
113	Microwave Impedance of Thin-Film Superconductor–Normal Metal Hybrid Structures with a High Conductivity Ratio. Physics of the Solid State, 2019, 61, 1675-1681.	0.2	0
114	Microstructure and Density of Mo Films in Multilayer Mo/Si Mirrors. Journal of Surface Investigation, 2019, 13, 8-13.	0.1	0
115	Atomic Force Microscopy Examination of Elementary Processes in Metalorganic Compound Hydride Epitaxy of GaAs-Based Nanoheterostructures. Technical Physics, 2020, 65, 791-794.	0.2	0
116	The Magnetoelectric Effect in Ferroelectric/Ferromagnetic Film Hybrid Systems with Easy-Plane and Easy-Axis Anisotropy. Technical Physics, 2020, 65, 1832-1836.	0.2	0
117	Modification of the Ratio between sp2- to sp3-Hybridized Carbon Components in PECVD Diamond-Like Films. Semiconductors, 2020, 54, 1047-1050.	0.2	0
118	Effect of the Chloropentafluoroethane Additive in Chlorine-Containing Plasma on the Etching Rate and Etching-Profile Characteristics of Gallium Arsenide. Semiconductors, 2021, 55, 865-868.	0.2	0